Transitions in morphologies, fluid regimes and feeding mechanisms during development of the medusa *Lychnorhiza lucerna*

Renato M. Nagata[1,2,6*], André C. Morandini[1,2], Sean P. Colin[3,4], Alvaro E. Migotto[1,2] & John H. Costello[2,3]

[1]Departamento de Zoologia, Instituto de Biociências, Universidade de São Paulo, Rua do Matão, trav. 14, n. 101, 05508-090, São Paulo, SP, Brazil. renatonagata@gmail.com

[2]Centro de Biologia Marinha, Instituto de Biociências, Universidade de São Paulo, 11600-970, São Sebastião, SP, Brazil.

[3]Marine Biological Laboratories, Woods Hole, Massachusetts, United States of America.

[4]Marine Biology and Environmental Science, Roger Williams University, Bristol, Rhode Island, United States of America.

[5]Biology Department, Providence College, Providence, Rhode Island, United States of America.

[6]*Present address:* Instituto de Oceanografia, Universidade Federal do Rio Grande, Av. Itália, km 8, 96203-000 Rio Grande, RS, Brazil

*Corresponding author: renatonagata@gmail.com

ABSTRACT

The early ontogeny of scyphomedusae involves morphological and functional transitions in body plans that affect the predators' propulsive and feeding strategies. We applied high-speed videography, digital particle image velocimetry (DPIV) and dye visualization techniques to evaluate alterations in swimming and feeding mechanisms during ontogeny of the rhizostome medusa *Lychnorhiza lucerna* Haeckel, 1880 (Scyphozoa, Rhizostomeae). During early ontogeny, the ephyral mouth lips develop into complex filtering structures along the oral arms. The viscous environments (Reynolds number <100) experienced by ephyrae constrain the feeding mechanisms that transport fluid during ephyral bell pulsations. In contrast, adult medusan fluid flows are dominated by inertial forces and bell pulsations effectively transport fluids and entrained prey toward the oral arms. The oral arm surfaces are covered by motile epidermal cilia that drive these entrained flows through filtering gaps in the oral arms where food particles are retained. In addition to this process within the oral arms, vortices generated during bell pulsation flow downstream along the outside of the medusae and continuously transport prey toward the exterior oral arm surfaces. Although calanoid copepods are capable of escape velocities that greatly exceed *L. lucerna*'s feeding current speeds, copepods often fail to detect the predator's feeding currents or inadvertently jump into medusan capture surfaces during failed escape attempts. Consequently, the comparatively weak predator feeding currents successfully capture a portion of the copepods encountered by swimming medusae. These results clarify the processes that enable rhizostome medusae to play key roles as consumers in tropical and subtropical coastal environments.

KEY WORDS: Feeding behavior, Foraging mode, Filter-feeding, Jellyfish, Gelatinous zooplankton.

INTRODUCTION

Many planktonic predators feed as ambush predators (*e.g.* hydromedusae and siphonophores), which remain stationary most of the time, waiting for the collision of prey with their expanded capture surfaces (*e.g*. marginal tentacles) (Costello et al. 2008). In contrast, most scyphozoan medusae (~200 spp.) are filter-feeders that utilize nearly continuous swimming to encounter and capture prey. Periodic bell pulsations of scyphomedusae produce vortices that both generate forward thrust and direct the surrounding fluids downstream (Dabiri et al. 2005). This flux promotes encounter of prey with a predator's feeding structures – the tentacles and the oral arms (Costello & Colin 1994, Dabiri et al. 2005, Acuña et al. 2011).

The utilization of swimming to pump water through feeding structures for prey capture is a widespread mechanism among medusae possessing oblate umbrellas (Costello et al. 2008). Nevertheless, specific prey retention patterns vary due to the diversity of body architectures and prey capture structures (tentacles, oral arms) that trail in the wake behind pulsing scyphomedusan bells. All of these structures are armed with clusters of nematocysts, which discharge and retain prey before they are transported to the mouth opening. The shape and the position of prey capture structures vary widely among scyphomedusan groups. While medusae of Coronate and Semaeostomeae capture prey with their tentacles and oral arms, species of the derived clade Rhizostomeae (~90 spp.) lack marginal tentacles, and capturing prey solely on highly specialized filtering oral arms (Costello & Colin 1995).

The specialized morphology of adult rhizostome medusae contrasts with the simple body plan of the initial medusan developmental stage, the ephyrae, which are very similar among distinct scyphozoan lineages (Russell 1970). The early growth of

rhizostome ephyrae involves dramatic size changes that are accompanied by transitions to adult morphologies and feeding strategies. Ephyrae are typically only millimeters in diameter, whereas their adult counterparts usually have larger body size (typically > 1cm bell diameter), with some species attaining bell diameters of 2 m and wet weights of ~200 kg (Kawahara et al. 2006). This means that some species undergo a size transition encompassing three orders of magnitude during their planktonic life. Such change imposes functional demands on organisms, since shifts in fluid regimes (*i.e.* Reynolds number, Re) may alter the functions of body structures (Koehl et al. 2001, Koehl 2004, Higgins et al. 2008, Feitl et al. 2009). These developmental changes in jellyfish dimensions necessitate a transition from fluid environments dominated by viscous forces during ephyral swimming to inertial forces for most adult scyphomedusae.

The feeding strategies by rhizostome medusae have important implications for marine trophodynamics, since these medusae are frequently dominant components of tropical and subtropical marine planktonic ecosystems (Kawahara et al. 2006, Schiariti et al. 2008), with some species (*e.g. Rhizostoma pulmo*) occurring in high densities even in temperate areas (Kramp 1970, Russell 1970). These animals do not merely drift within water masses but are capable of oriented swimming relative to the water currents (Fossette et al. 2015) and complex foraging movements (Hays et al. 2011). Although general aspects of swimming and feeding mechanisms have been described for several rhizostome species (Costello & Colin 1994, D'Ambra et al. 2001, Santhanakrishnan et al. 2012) the exact feeding modes are poorly known in the group, as well as the development of this mechanism during ephyral growth. A mechanical understanding of fluid manipulations by these medusae and the reactions of their prey to these fluid manipulations is important for prediction of resulting planktonic trophic interactions.

93 *Lychnorhiza lucerna* Haeckel, 1880 is the most abundant rhizostome in south
94 and southeast Brazil, occurring throughout the year with seasonal population increases
95 (Morandini 2003, Nogueira Jr 2006). Although these blooms represent a nuisance to
96 shrimp trawlers in Brazil (Nagata et al. 2009) and northern Argentina (Schiariti et al.
97 2008), information on the trophic role of this medusae species is incomplete. The goals
98 of this study were: *i*- to describe sequential morphogenesis of ephyral lips into adults
99 oral arms; *ii*- to analyze parameters of swimming, bell kinematics, and animal-fluid
100 interaction throughout development; *iii*- analyze the fluid motions around swimming
101 medusae and the interaction of wake vortex rings with feeding structures; and *iv*- to
102 describe predator-prey interaction of *L. lucerna* and calanoid copepods. We focused
103 only on interactions between *L. lucerna* and calanoid copepods since these are the main
104 food items for this species (Nagata 2015). We hypothesized that: i- the development
105 from ephyral to the adult body plans entails a transition in fluid regimes (*i.e.* Re) that
106 affects both propulsive and feeding strategies; and ii- the sensitivity of calanoid
107 copepods to small hydrodynamic disturbances, coupled with their rapid escape
108 responses, influence predator capture success.

109 **MATERIAL AND METHODS**

110 **Sampling and cultivation of medusae**

111 We collected medusae of *Lychnorhiza lucerna* with hand nets in surface waters
112 of Cananéia Estuary (25º04' S, 47º52'W), Southeast Brazil, in March and April 2013.
113 Animals were packed in plastic bags with local seawater and immediately transported to
114 CEBIMar-USP in São Sebastião, São Paulo state, where they were kept inside 5 m^3
115 containers, with filtered (3 µm) running seawater at ambient temperatures (20-24ºC),
116 and fed daily with natural plankton collected with a 200 µm net. Medusae ranged in bell
117 diameter (distance from opposite rhopalia) from 3−7 cm. Ephyrae and young medusae

(0.5–3 cm bell diameter) were reared in laboratory from polyps kindly provided by Dr Agustin Schiariti (INIDEP), from the region of Clamercó, NE coast of Argentina. We maintained polyps following protocols of Jarms et al. (2002) (in the dark, fed weekly, at constant temperature of 22º C and salinity of 20). Ephyrae were reared in *planktonkreisels* similar to those described by Raskoff et al. (2003) and fed daily with freshly hatched *Artemia* sp. nauplii.

Ephyral development and formation of the filtering oral arms.

To describe the serial development of oral arms in *L. lucerna*, we analyzed recently (one day old) released ephyrae (N=10) under a stereomicroscope and photographs were taken with a digital camera (Nikon SMZ1000). Ephyrae were anesthetized with $MgCl_2$ (3.5% in seawater) and photographed daily during the first 20 days, when the animal undergoes a rapid morphological transition, and thereafter, every 5 days, during a total of 2 months after release. We focused our analyses on morphological development of ephyral manubria into the eight filtering oral arms of adults. In order to compare the dimensions of capture structures (*i.e.* digitata),of *L. lucerna's* with those of other medusae of Rhizostomeae, measures of digitata length, bulb, stem width and spacing between consecutive digitata were measured from pictures of live animals.

Video Recordings

We placed animals within rectangular aquariums with dimensions of 30 x 40 x 10 cm (width x height x depth) containing filtered seawater. We used three imaging set-ups for our analyses: *i*- laser sheet illumination for swimming and bell kinematic analyses and for the digital particle image velocimetry (DPIV) quantification of the velocity fields surrounding the animal (*e.g.* Colin et al. 2013); *ii*- side illuminated

142 fluorescein dye visualization of flow, for a qualitative description of the interaction
143 between the vortex ring and the inner structures of oral arms; and *iii*- high magnification
144 collimated light illumination for predator-prey interactions and prey capture
145 visualization.

146 The laser sheet was generated using a 530-nm wavelength laser. White light for
147 fluorescein dye and collimated light techniques was generated using light emitting
148 diodes (LEDs). Videos were recorded at 1000 frames s^{-1} using a high-speed digital
149 video camera (FASTCAM SA3; Photron). Videos for DPIV were recorded with filtered
150 seawater, seeded with hollow glass spheres (10 µm). A laser sheet illuminated a two-
151 dimensional plane of fluid and data were collected when the center of the medusa bell
152 was bisected by the laser plane, following Colin et al. (2013). Medusae were left
153 swimming from the bottom to the top of the vessel for at least 3-5 cycles of bell
154 pulsation and the video sequences of a few seconds were recorded. For the fluorescein
155 dye technique, a syringe was used to add the dye near the umbrella margin of swimming
156 medusae. The formation of starting vortex rings and their movements towards the
157 structures of the oral arms were recorded. For videos sequences of predator-prey
158 interactions, medusae were placed swimming around calanoid copepods, which were
159 collected at the São Sebastião Channel, with a 200 µm net. We added only a few
160 copepods inside the aquariums in order to avoid mutual interference between prey
161 during encounters with the medusa. Encounters of *L. lucerna* with copepods of *Acartia*
162 spp. and *Temora turbinata,* were recorded at 1000 frames s^{-1}. We analyzed frame by
163 frame sequences with copepods with unbroken pairs of first antennae, and escaping
164 responses in a focused plane perpendicular to the camera. The complete escape
165 movement comprised the recoil of the first pair of antennae and the escaping jumps
166 through the reopening of the first antennae.

Data Analysis

Bell and swimming kinematics were analyzed using ImageJ software (NIH). All measurements were taken at intervals (t) of 0.01 s for ephyrae and young medusae, and of 0.02 s for larger animals. Alterations in bell shape were measured by the fineness ratio, f, according to (Costello & Colin 1994) as:

$$f=H/D,$$

where H = bell height, and D= bell diameter.

The contraction angle (c) of the bell margin was measured by the difference between the angle of bell margin relative to the animal's axis of symmetry at the maximum relaxation phase (θ), and at the maximum contraction phase (θ'), as:

$$c=\theta - \theta'.$$

The scheme of the measurements is presented at Fig. 1a.

Figure 1

Distance traveled, m, was measured from sequential changes in position of the anterior most point of the exumbrellar surface over t intervals. The final and initial position on axes X and Y of the screen were measured using ImageJ software, and the displacement was calculated by applying the Pythagorean theorem:

$$m=\sqrt{(Xf-Xi)^2+(Yf-Yi)^2},$$

where Xf and Yf are the final and Xi and Yi the initial position at each axes. Medusa swimming velocity u for a time interval (t) was calculated as:

$$u= m/t$$

189 Mean swimming velocity u_m was calculated as mean u during three successive complete
190 bell contraction cycles.

191 Reynolds number (*Re*) was calculated as:

192 $Re = D*u/v$,

193 where u is the medusa velocity and v is the kinematic viscosity of seawater at 20ºC.

194 For measurements of flow velocities with digital particle image velocimetry
195 (DPIV), we used the software package (DaVis, Lavision) that analyzes sequential video
196 frames using a cross-correlation algorithm. The frame of reference for all images was
197 the fixed image field through which the animals moved. Velocity fields were integrated
198 over periods of 3-5 frames (3-5 ms), depending on animal size and velocity, in order to
199 allow sufficient particle motion but negligible animal motion during each image pair.
200 Image pairs were analyzed with shifting overlapping interrogation windows of
201 decreasing size (64X64 pixels then 32X32 pixels). This analysis generated velocity
202 vector fields around the swimming medusae (Colin et al. 2013). We defined feeding
203 currents as the flows generated by bell pulsations, in the form of vortex rings, which
204 collided with the medusa's prey capture surfaces on their oral arms. We measured the
205 maximum velocities of feeding currents u_f along the full cycle of bell relaxation and
206 contraction by DPIV. Oblate cruising medusae are highly dependent on locally
207 generated flow current to capture prey (Costello & Collin 1994, Dabiri et al. 2005). To
208 achieve a better visualization on how directed flow interacted with oral arms, we
209 calculated fluid velocities along transects at different locations adjacent to the oral arms.
210 At these transects, velocities of fluid motion were decomposed into axial velocities, of a
211 vertical (Y) and a horizontal (X) component. Thus, we could evaluate the importance of
212 fluid transport generated by bell pulsation relative to the position of distal surfaces of

prey capture on oral arms. In order to test whether changes in medusae body size were related to changes on biomechanics parameters (*e.g*. fineness ratio *f*, contraction angle *c* swimming velocity *u, Re*), these last were used as dependent variables against bell diameter in linear and non-linear regressions analyses. Before all regression analyses, the assumptions of normality and homogeneity of variances were tested and when necessary, data were log10-transformed.

Encounters of *L. lucerna* with copepods *Acartia* spp. (N=38) and *T. turbinata* (N=40) were characterized for medusae of sizes between 0.6 to 3 cm of bell diameter (N=4). Parameters of encounters were quantified such as frequency of escape response, prey size (mm), distance from predator where escaping reactions starts (mm), maximum velocity of escape ($mm*s^{-1}$), distance traveled during escapes (mm), turning angles before escape (degree), escape angles relative to predators feeding structures (degree), and duration of escapes (s).

Prey capture maps

In order to generate a map of prey captures on the oral arms, we quantified prey captures along the surface of oral arms of medusae (n=5). Animals were incubated in a container with filtered (3 µm) seawater and *Artemia* spp. nauplii for 2 minutes. After incubation, individuals were carefully removed and preserved in a 4% formaldehyde solution in seawater. We quantified the number of nauplii in four oral arms (of a total of 8 oral arms) of each individual under a stereomicroscope. The oral arm surface is comprised of three wings (two external and one internal), each wing was subdivided into regions (5 for the external and 6 for the internal wing) according to the distance from the bell (Fig. 1B). In order to estimate prey capture per unit area (cm^2), we estimated the oral arm surface area as the surface of a truncated cone as:

237 $$S_{ob} = \pi(r_1+r_2)\sqrt{h^2+(r_1-r_2)^2},$$

238 Where r_1 = large radius, r_2 = small radius, and h = section height, according to Fig. 1B.
239 ANOVA analyses were applied to test differences in captures between the three oral
240 wings and between regions on each oral wing. Normal distribution (Shapiro-Wilk's *W*
241 test) and homogeneity of variances (Bartlett test) were tested before these analyses and
242 Kruskal-Wallis tests were used if necessary.

243 **RESULTS**

244 **Morphological transition and the development of the filtering oral arms.**

245 Recently released *Lychnorhiza lucerna*'s ephyrae (3-5 mm of bell diameter)
246 typically have a flat bell, a margin with gaps between the 8 lappets, and a cross-shaped
247 central mouth (Fig. 2 A). Three to five days after release, the margin of the mouth
248 developed many finger-like projections, armed with terminal nematocysts clusters,
249 called *digitata* (Fig. 2 B). As bell diameter reached 12 mm, gaps between adjacent
250 lappets were filled and bell margins became continuous. In 12-20 day old ephyrae (8–20
251 mm) the tips of the cross-shaped mouth branched to the eight oral arms (Fig. 2C). In 20-
252 30 day old ephyrae (10–25 mm)**,** as oral arms develops radially, many lateral folds arose
253 along their surfaces (Fig. 2D). These folds developed laterally to cover spaces between
254 adjacent oral arms (Fig. 2D). Still, the distal region of oral arms branched further and
255 gave rise to the two external wings (*E1* and *E2,* Fig. 2E) and the central mouth aperture
256 was obliterated. The oral arm transitioned to a filtering surface, and the branching
257 pattern of oral arms edges then contained many gaps of circular-polygonal shape, which
258 structurally resembled a sieve (Fig. 2F). Two months after release (~2 cm bell diameter)
259 and throughout further development, the oral arms elongated distally and became
260 increasingly cone-shaped (Fig. 2G). The oral arms possessed a complex three-

dimensional structure, with a highly ramified edge that operated as a continuous suctorial surface (Fig. 2H). Captured prey were transferred to the oral arm canal system through many millimeter-width pores of the canal inlets (Fig. 2H).

Figure 2

Ontogenetic changes on bell kinematics and pulsation mode

The bell outline had differences on both contraction and relaxation phases between ephyrae and adult animals (Fig. 3). A larger portion of the ephyrae bell (from the bell margin to near the bell apex) moved during both contraction and expansion (Fig. 3, A and C). In ephyrae, the expansion movement led to a partial inversion of the bell (Fig. 3A). In adults only the distal portion, close to the bell margin moved, whereas the region representing ~50% of the bell center-bell margin distance remained largely immobile (Fig. 3, B and D). The contraction of bell in ephyrae is 2x faster than the relaxation, and 4x faster than the bell contraction of adults (Fig. 3).

Figure 3

The fineness ratio (*f*) and bell contraction angle (*c*) throughout bell pulsation cycle also changed along the transition from ephyra to adult stages (Fig. 4). For ephyrae the average *f* was lower (*f* = 0.2–0.5) and increased up to dimensions larger than ~2 cm of bell diameter, when *f* reached a relatively stable adult bell shape (*f* = 0.5–0.8) (Fig. 4). Similarly to *f*, the bell contraction angle (*c*) also changed during early development with wider movements of contraction and expansion in ephyrae (*c*=48–78 degrees), whereas *c* decreased and reached a relatively constant level at diameters above ~2 cm (*c*=28 to 35 degrees) (Fig. 4).

Figure 4

287

288 *L. lucerna* undergoes a transition in its fluid environment (as Reynolds numbers,
289 *Re*) during growth. In ephyrae with diameters less than 1.5 cm ($\log_{10}$ bell diamameter
290 <1.17) , maximum *Re* were <325 ($\log_{10} Re$<2.5) and predominantly near 50
291 ($\log_{10} Re$~1.7) (Fig. 5 A). For *Re* in the range of 1<*Re*<100, where ephyrae swiming
292 predominantly ocurred, both viscous and inertial forces were important. In contrast, the
293 fluid enviroments of larger medusae, diameters greater than 2.5 cm ($\log_{10}$ bell diameter
294 <1.4), were characterized by higher mean and maximum *Re* of >300 and >800
295 respectively ($\log_{10} Re$ <2.5 and 2.9). In this range, fluid environments were dominated
296 by inertial forces (Fig. 5).

297 In order to understand the effect of body size on swimming kinematics and on
298 the strength of feeding currents, we quantified the mean (u_m) and maximun (u_{max})
299 swimming velocities and maximum velocities of feeding currents (u_f) produced by bell
300 pulsations. Swimming (u_m, u_{max}) and feeding current velocities increased linearly with
301 increases in bell diameter (Fig. 5 B). Peak feeding current velocities, u_f, in small
302 medusae (bell diameter <2 cm) were similar to peak swimming velocities, u_{max} (paired
303 t-test, t(4)=1.84, p=0.14). However, in larger medusae, u_f became increasingly greater
304 than u_{max}. The slope of u_f linear regression was 1.29, while for u_m and u_{max} it was 0.35
305 and 0.61 respectively (Fig. 5 B).

306 **Figure 5**

307 **Fluid transport to prey capture surfaces**

308 Analysis of the digital image particle velocimetry (DPIV) revealed the manner in
309 which the flux of fluid generated during bell pulsations interacted with prey capture
310 surfaces on oral arms. The DPIV revealed the formation of starting and stopping
311 vortices during contraction and relaxation phases, respectively. At maximum

312 contraction phase (Fig. 6, T=0), the medusa was about to start bell expansion. The
313 expansion of the bell resulted in the entrainment of fluids surrounding the exumbrella,
314 with flow directed towards the subumbrella as a stopping vortex (Fig. 6, T= 50 %).
315 With maximum bell expansion (Fig. 6, T= 100%), fluid entrainment decreased and
316 contraction was initiated (Fig. 6, bottom). Between T=0 and T=50% (Fig. 6, bottom),
317 fluid surrounding the exumbrella circulated into a starting vortex. Maximum fluid
318 velocities ($u_f \approx 9$ cm*s^{-1}) were found near the bell margin at 50% contraction (t=0.45 s).
319 After the maximum contraction of bell, the water displacement kept adding energy to
320 the rotation of vortex (see supplemental movie 1).

321 Fig 6

322 Fluid transport towards the prey capture surfaces were evaluated as the X axial
323 velocity cm*s^{-1} (see methods) along transects on oral arms (Fig. 7). Fluid transport from
324 the vicinities of exumbrella towards medusa's axis of symmetry (inside the bell and oral
325 arms) are represented as negative values, whereas transport from internal region to
326 outside are positive values. In ephyrae, the highest velocities occurred immediately
327 below bell margin, at 25 and 50 % of the period of total contraction. Velocities rapidly
328 attenuated to between 75 and 100% of the contraction period. Because of this rapid
329 dissipation, fluid velocities at the distal prey capture surfaces were nearly zero, or
330 slightly positive. During bell expansion, fluid was also transported towards the animal's
331 symmetry axis, but at slower velocities than during contraction. Fluid transport (as X
332 velocities) produced during both bell contraction and expansion were less effective at
333 producing fluid transport towards prey capture surfaces in ephyrae (Fig. 7 A).

334 In adults (>26 mm), similarly to ephyrae, the transport of fluids towards the
335 medusa's axis of symmetry occurred during both bell contraction and expansion, but
336 peak velocities were found between 50 and 100 % of total contraction period (Fig. 7 B).

337 The highest fluid transport velocities were found in the region of the oral disk, between
338 the bell margin and the beginning of the prey capture surfaces (Fig. 7B). In contrast to
339 ephyrae, starting vortices of adults did not immediately dissipate, but instead, moved
340 distally away from bell margin and continued to transport fluids towards prey capture
341 surfaces. During both pulsation phases, a small velocity peak occurred at the end of oral
342 arms of adults. This secondary peak, typically of a magnitude nearly half the peak bell
343 margin velocity, represented the remnants of starting vortices generated during the
344 previous bell pulsation cycle, propagated away from the bell with continued transport of
345 fluid and entrained particles towards the oral arm tips (Fig. 7B). At any one time, the
346 most recent starting vortex as well as the remnant starting vortex from the previous bell
347 contraction cycle traversed the length of adult oral arm exterior surfaces.

348 **Figure 7**

349 Although the DPIV technique provides high resolution fluid velocity
350 information, it permits limited insight into flows within the oral arm structures
351 themselves. The fluorescein dye technique allowed the visualization of fluid transport
352 from internal surfaces of oral arms through the prey capture structures. As the medusae
353 expanded its bell, fluid was transported just below bell margin to refill the subumbrellar
354 cavity (Fig. 8A). During bell contraction, a starting vortex was formed and the border of
355 the vortex ring encountered the oral arm (Fig. 8 B). During the next bell expansion, and
356 formation of its associated stopping vortex on the subumbrellar surface, the previous
357 starting vortex rotated downstream along the exterior oral arm surfaces (Fig. 8C). As the
358 next contraction began, the fluid previously transported to the inner region of oral arms
359 declined in velocity and diffused outward through the distal ends of oral arms (Fig. 8D).

The water entrained towards the subumbrellar surface traveled past the epidermal layer, which is covered by many motile cilia (supplemental movie 2). These cilia transported water distally toward toward the oral arms. The internal surfaces of the oral arms, including the *digitata*, are also covered by epidermal cilia which have movements of identical direction, but apparently in a non-synchronized beating pattern (supplemental movie 2). This ciliary beating generated currents that transport fluids from the interior spaces within the oral arms to the tips of digitata where capture by nematocysts occurs. The digitata bear clusters of nematocysts (located on the digitata tips and bases) which retain prey before ingestion. The oral arm edges operate as filtering surfaces as vortices move along the edge surfaces. Simultaneously, fluid passes from regions inside the oral arms outwards through the polygonal gaps formed during oral arm development (Fig. 2F).

Figure 8

Prey escape from medusan feeding currents

Prey responses to swimming *L. lucerna* medusae strongly influenced predator capture success. All encounters between *Acartia* spp. (N=38) and *L. lucerna* medusae resulted in escape responses. However, 17% of encounters between *Temora turbinata* (N=40) and *L. lucerna* medusae did not elicit evasive jumps by copepods and those *T. turbinata* were then transported past the bell margin by medusan feeding currents toward the oral arms. Several sequences of copepod-medusa interactions are shown in supplemental movie 3. Table 1 summarizes copepod escape parameters during interactions with swimming *L. lucerna* medusae. For *Acartia* spp., escapes were primarily double jumps of short duration (~0.03 s), whereas for *Temora turbinata*, escapes composed multiple jumps (~0.13 s), reaching greater total distances (~10.53 mm) (Table 1). The distance from a predator where copepods initiated escapes were

higher for *Acartia* spp., which initiated escapes on average at *c.a.* 5 body lengths (5.42 mm) from a predator, while *T. turbinata* often did not try to escape until drawn much closer to the predator (*c.a.* 1 body length before the escape response, Table 1, supplemental movie 3). *Acartia* spp. escaped at angles wider than 90° (94% of the escapes) relative to the predators feeding structures. In contrast, *T. turbinata* escape angles were more variable and escapes angles narrower than 60° were frequently recorded (27%).

Table 1

Depending on the location of where prey were transported, they became susceptible to capture by oral arms in different ways. When prey were transported to the interior of the oral arms, they frequently were confined in the spaces between oral arm wings. Prey then encountered digitata during navigation through the polygonal gaps in the oral arms (see supplemental movie 4). Prey were also vulnerable to capture when transported within starting vortex propagation along the exterior oral arm surfaces. Copepod escape angles were often inadequate for escape and resulted in their capture on oral arm surfaces (see supplemental movie 5).

Prey capture maps

In order to evaluate the relative importance of different regions of the oral arm structures for prey capture, we tabulated results of 5893 *Artemia* sp. nauplii that were captured on oral arms of 5 medusae. The absolute percentages of prey captures were significantly different between the different wings of the oral arms (ANOVA, $F_{2,12}$= 5.59, p<0.05), with higher captures on the external wing 2 in relation to the internal wing (Tukey´s Test p<0.05) (Fig. 9). There were no significant differences between regions (1–6) along the internal wing of the oral arm (ANOVA, $F_{5,24}$=2.34, p=0.07).

However, regions along the length of external wing 1 (ANOVA, $F_{4,20}$= 8.07, p<0.001) and external wing 2 (ANOVA, $F_{4,20}$=10.73, p<0.001) did exhibit significantly more captures along regions "3" and "4" than the region "6" for external wing 1 and lower captures at region "6" than any other region, for the external wing 2 (Tukey's Test p<0.05). Differences in the absolute number of captures on different oral arm wings were related to differences in areas of the oral arm wings because, when normalized by the area available for capture, there were no significant differences in capture rates between the three wings (Kruskal-Wallis, $\chi^2(2)$= 5.79, p=0.06).

DISCUSSION

Morphological transition and the development of the filtering oral arms

Similarly to other members of the Rhizostomeae, *Lychnorhiza lucerna* undergoes a series of morphological changes in its feeding apparatus during early development (Uchida 1926, Sugiura 1966, Holst et al. 2007, this study). Scyphozoan ephyrae lack specialized feeding structures (*e.g.* tentacles and oral arms), and capture prey along the subumbrellar surface and marginal lappets (Sullivan et al. 1997, Higgins et al. 2008). Recently released *L. lucerna* ephyrae rapidly develop digitata along mouth edges (Fig. 2B), which are the first specialized capture structures. In the viscous fluid environment of ephyrae (Re <10^2), momentum transfer of flow is minimal and bell pulsations are less effective in producing flows through the digitata (Fig. 7A). As medusae grow, inertial forces become increasingly dominant and bell pulsations become effective for pumping fluid along the oral arm surfaces. Adult medusae develop structures within the oral arms that contain numerous filtration gaps (Fig. 2F). This developmental transition occurs during a shift in hydrodynamic regime that includes higher Re flows and more fully developed vortex generation at the bell margin. The

434 larger vortices strongly influence prey transport and the locations of prey capture. These
435 transitions in morphology and feeding mechanics determine a biomechanical framework
436 within which predation by rhizostome ephyrae and young medusae occurs.

437 Changes in bell shape during early development in *L. lucerna* affected both bell
438 pulsations patterns and the propulsion mode. The change of an oblate ephyral bell
439 (fineness ratio f=0.2–0.4) into a prolate bell (f=0.5-0.8) reduces drag by streamlining,
440 which increases swimming efficiency in an inertially dominated fluid environment
441 ($Re<10^3$) (Colin et al. 2013). In ephyrae, the longer stroke lengths of bell pulsation
442 (Figs. 3 & 4 B) are characteristic of drag-based paddling (Blough et al. 2011), which is
443 a common strategy for animals living in lower *Re* (Vogel 2003, Higgins et al. 2008,
444 Feitl et al. 2009). In this propulsive mode, forward thrust ceases after the power stroke
445 and the wider strokes enable higher thrust production, since forward thrust is directly
446 related to the stroke length (Vogel 2003, Blough *et al*. 2011). In contrast, swimming by
447 adults involves movements primarily by the bell margin. These adult bell pulsations
448 produce two opposite rotational vortices, which generate forward thrust and transport
449 prey to prey capture structures (Dabiri et al. 2005). These results demonstrate that the
450 transition in fluid environments accompanying development was accompanied by
451 alterations in both propulsive and feeding strategies of *L. lucerna*.
452

453 **Fluid transport to prey capture surfaces**

454 Swimming (u_m and u_{max}) velocities increased with the medusa size. However,
455 feeding current velocities (u_f) increased more rapidly with bell size than did swimming
456 velocities. Higher feeding current velocities are important for the dietary niche because
457 they allow the transport of more evasive prey (Costello & Colin 1994). Maximum u_f
458 were found at the interface between stopping and starting vortices, at ~50% of bell

459 contraction (Fig. 6). Dabiri et al. (2005) argued that momentum flux increased at the
460 interfaces of these vortices. These vortex interactions increase u_f, which enhances fluid
461 transport as well entrainment of more evasive prey.

462 Although the production of feeding currents via bell pulsations is widely used
463 among large medusae (Colin & Costello 1995), the shape and positioning of feeding
464 structures in relation to swimming vortices vary between medusan species. This may
465 result in distinct modes of prey capture and prey selectivity. In medusae with marginal
466 tentacles, like the scyphozoan *Aurelia* sp. and the hydrozoan *Aequorea victoria,* tentacles
467 lie in the center of the starting vortex (Dabiri *et al.* 2005, Lipinski & Mohseni 2009).
468 Nevertheless, rhizostome medusae lack marginal tentacles and have a great diversity of
469 bell morphologies and oral arms shapes, which may generate distinct modes of
470 interactions between vortices of bell pulsation and oral arms (Fig. 6). In *L. lucerna,* only
471 the edge of the vortex contacts oral arms while the center of vortex moves freely
472 downwards, outside the oral arm surface and entrains surrounding fluids towards the oral
473 arms. This pattern is different from that of the rhizostome *Cassiopea* sp., which has a
474 flatter bell and oral arms that extend far from the animal's symmetry axis. The entire
475 vortex (not only its inside edge) translates through the oral arms of *Cassiopea* sp. (Hamlet
476 *et al.* 2011, Santhanakrishman *et al.* 2012).

477 Velocity fields determined by DPIV demonstrated that vortices transported
478 fluids to the oral arms, where particles were retained. For *L. lucerna,* a division of the
479 entrained fluids occurs so that only a small portion of the starting vortex is channeled to
480 the inner oral arms (Figs. 6-8), whereas the majority of the starting vortex travels
481 downstream along the exterior of the oral arms. This downstream propagation of the
482 starting vortex enables fluid transport along the external wings of the oral arms (Fig. 7

B) and transport of prey to the external oral arm wings (Fig. 9) where they are captured by digitata lining the exterior oral arm wings.

Unlike the fluid that flows along the exterior oral arm surfaces, the fluid that is transported into the inner oral arms (Fig. 6) becomes confined within the cavities formed by the three wings of the oral arms. This water is then pushed from the interior of the oral arms through the filtering gaps to the oral arm exterior by cilary currents generated along the epidermal surfaces of the highly complex (Fig. 2G-H) oral arm body. Due to the size of these gaps, (Fig. 2E-F) smaller particles can pass freely to the outside. However, larger particles are trapped and retained by nematocysts lining the digitata. The similarity of digitata dimensions among rhizostome medusae (Fig. 10) suggests that patterns found for *L. lucerna* may be more widely applicable to other rhizostome medusae.

Figure 10

Prey escape from medusan feeding currents

Calanoid copepods possess well developed escape responses to predators (Burdick et al. 2007, Yen 2010, Buskey et al. 2011) and might be expected to elude the comparatively slow feeding current velocities of *L. lucerna.* The copepods *Acartia* spp. and *Temora turbinata* are the dominant co-occurring mesozooplankton with *L. lucerna* (Nagata & Morandini in prep.) and are capable of escape swimming velocities between 10 and 55 cm s^{-1} (Table 1). These escape velocities are up to 5 times faster than maximum velocities of *L lucerna'*s feeding currents (u_f<10 cm*s^{-1}; Fig. 5B). Although the robust pulsations of rhizostome medusae produce comparatively rapid feeding currents relative to other scyphozoans (*e.g. Aurelia* sp. <3 cm*s^{-1} and *C. quinquecirrha* ~5 cm*s^{-1} for individuals <8 cm of bell diameter, D'Ambra et al. 2001 and Santhanakrishnan et al. 2012, respectively), these feeding current velocities may still be

508 insufficient to exceed escape velocities of co-occurring copepods. The few field data on
509 rhizostome feeding habits provide equivocal evidence that calanoids may both avoid
510 predation (Larson 1991, Álvarez-Tello et al. 2015), or be captured in similar proportions
511 to environmental densities (Fancett 1988, Nagata 2015).

512 On the other hand, it is important to emphasize that prey items of limited escape
513 ability may also avoid predation by failing to elicit a retention response on a predator´s
514 capture structures. Several sequences (supplemental movie 6) demonstrated the absence
515 of capture reaction by the *digitata,* especially in the case of contact with diatoms
516 (*Coscinodiscus* sp.). Further studies are needed to better characterize details of post
517 encounter between medusae and their prey, since retention efficiency is among the main
518 parameters governing prey capture success (Riisgård 1988; Jaspers *et al*. 2011).

519 How do these medusae succeed at capturing copepods despite the capability of
520 copepods to simply swim out of a medusa's feeding current? Actually, most encounters
521 between *L. lucerna* and copepods that we observed resulted in escape by the copepod
522 and indicated low capture efficiencies by the medusae on calanoid copepods. However,
523 we also found circumstances that favored successful capture of copepods by medusae.
524 During some predator-prey encounters, copepod prey failed to detect the medusan
525 predator's feeding current and no escape response occurred prior to contact between
526 predator and prey. In 17 % of encounters, *T. turbinata* did not react within flows created
527 by *L. lucerna* and were subsequently transported by predator feeding currents. In
528 contrast, *Acartia* spp. were more reactive and initiated evasive jumps at distances about
529 five times greater from *L. lucerna* than did *T. turbinata* (Table 1). Such a difference in
530 reactivity between species is consistent with recorded shear threshold sensitivities, for
531 which *Acartia* spp. appears to respond to shear deformations about five times smaller
532 than *Temora* sp. (Colin et al. 2010). *Acartia* spp. generally avoided medusae by

escaping feeding currents before reaching a medusa's bell margin, whereas *T. turbinata* allowed transport within medusan feeding currents and sometimes appeared not to detect an approaching medusa. A second potential source of copepod capture was observed to occur after a copepod appeared to detect the feeding current of a medusa but subsequently made a high-speed escape jump into, rather than away from, the medusa. Such "wrong direction" escape movements can occur because, as documented with artificial hydrodynamic disturbances (*e.g.* Buskey 2002), copepods do not always reorient with reference to a hydrodynamic cue prior to escape jumping. The high amount of vorticity within medusan feeding currents may further obscure the hydrodynamic directionality that is most favorable for a copepod escape jump. *Acartia* spp. performed escape jumps primarily in the opposite direction of medusan feeding current flows and thereby avoided entrainment within feeding currents. On the other hand, the narrower escape jump angles (<60º) in 27% of the encounters with *Temora turbinata* made them vulnerable to feeding current transport toward the oral arms (Figs. 6 & 7). Escape jumps by *T. turbinata* sometimes inadvertently led the prey towards the oral arms and resulted in capture (supplemental movie 5). Thus, due to mismatches in detection thresholds or escape directions, medusae may capture rapidly swimming prey despite the disparities between medusan feeding current and prey escape velocities. Thus, although our starting hypothesis that calanoid copepods would be sensitive to hydrodynamic disturbances created by medusae and subsequently escape, requires qualification. *Acartia* spp. did generally escape and *Temora turbinata* often escaped. However, failure to detect the medusan predator and mis-directed escape efforts resulted in copepod captures by *L. lucerna*. The frequency with which these interactions occur in nature influences the ability of these medusae to exploit a wide range of available prey within plankton communities.

ACKNOWLEDGEMENTS

The study was partially funded by grants 2011/00436-8, 2013/19478-8, and 2014/00824-6 São Paulo Research Foundation (FAPESP), and CAPES PROEX. The study is a contribution of NPBioMar, USP. We thank the Oceanographic Institute of the University of São Paulo (IO-USP) and Centro de Biologia Marinha (CEBIMar-USP) for providing facilities at the coast. We thank the staff of "Projeto Garoupas" (FAPESP 2011/50407-4) for allowing the use of tanks for cultivating our jellyfish. We also thank Ms Nilvea Ramalho de Oliveira, Mr Leandro Santos and Mr Elso Alves da Silva for their valuable support in cultivating the experimental animals.

BIBLIOGRAPHY

Acuña JL, López-Urrutia A, Colin S (2011) Faking Giants: The Evolution of High Prey Clearance Rates in Jellyfishes. Science 333:1627–1629

Álvarez-Tello F, López-Martinez J, Lluch-Cota DB (2015) Trophic spectrum and feeding pattern of cannonball jellyfish *Stomolophus meleagris* (Agassiz, 1862) from central Gulf of California. J Mar Biol Assoc UK doi: 10.1017/S0025315415001605

Blough T, Colin SP, Costello JH, Marques AC (2011) Ontogenetic Changes in the Bell Morphology and Kinematics and Swimming Behavior of Rowing Medusae: the Special Case of the Limnomedusa *Liriope tetraphylla.* Biol Bull 220:6–14

Burdick DS, Hartline DK, Lenz PH (2007) Escape strategies in co-occurring calanoid copepods. Limnol Ocean 52:2373–2385

Buskey EJ, Lenz PH, Hartline DK (2002) Escape behavior of planktonic copepods in response to hydrodynamic disturbances: high speed video analysis. Mar Ecol Prog Ser 235:135–146

Buskey EJ, Lenz PH, Hartline DK (2011) Sensory perception, neurobiology, and behavioral adaptations for predator avoidance in planktonic copepods. Adapt Behav 20(1):57−66

Colin SP, Costello JH, Hansson LJ, Titelman J, Dabiri JO (2010) Stealth predation and the predatory success of the invasive ctenophore *Mnemiopsis leidyi*. Proc Natl Acad Sci USA 107:17223–17227

Colin SP, Costello JH, Katija K, Seymour J, Kiefer K (2013) Propulsion in Cubomedusae: Mechanisms and Utility. PLoS ONE 8(2):e56393

Costello JH, Colin SP (1994) Morphology, fluid motion and predation by the scyphomedusa *Aurelia aurita.* Mar Biol 121:327–334

Costello JH, Colin SP (1995) Flow and feeding by swimming scyphomedusae. Mar Biol 124:399–406

593 Costello JH, Colin SP, Dabiri JO (2008) Medusan morphospace: phylogenetic
594 constraints, biomechanical solutions, and ecological consequences. Inv Biol 127:265-
595 290

596 D'Ambra I, Costello JH, Bentivegna F (2001) Flow and prey capture by the
597 scyphomedusa *Phyllorhiza punctata* von Lendenfeld 1884. Hydrobiologia 451:223–227

598 Dabiri JO, Colin SP, Costello JH, Gharib M (2005) Flow patterns generated by oblate
599 medusan jellyfish: field measurements and laboratory analyses. J Exp Biol 208:1257-
600 1265

601 Fancett MS (1988) Diet and selectivity of scyphomedusae from Port Phillip Bay,
602 Australia. Mar Biol 98:503–509
603 Feitl KE, Millett AF, Colin SP, Dabiri JO, Costello JH (2009) Functional Morphology
604 and Fluid Interactions During Early Development of the Scyphomedusa *Aurelia aurita*
605 Biol Bull 217:283-291

606 Fossette S, Gleiss AC, Chalumeau J, Bastian T, Armstrong CD, Vandenabeele S,
607 Karpytchev M, Hays GC (2015) Current-oriented swimming by jellyfish and its role in
608 bloom maintenance. Curr Biol 25:342–347

609 Hamlet C, Santhanakrishnan A, Miller LA (2011) A numerical study of the effects of
610 bell pulsation dynamics and oral arms on the exchange currents generated by the
611 upside-down jellyfish *Cassiopea xamachana*. J Exp Biol 214: 1911−1921.

612 Hays GC, Bastian T, Doyle TK, Fossette S, Gleiss AC, Gravenor MC, Hobson VJ,
613 Humphries NE, Lilley MKS, Pade NG, Sims DW (2011) High activity and Lévy
614 searches: jellyfish can search the water column like fish. P Roy Soc B: Biol Sci
615 279:465–473.

616 Higgins JE, Ford MD, Costello JH (2008) Transitions in Morphology, Nematocyst
617 Distribution, Fluid Motions, and Prey Capture During Development of the
618 Scyphomedusa *Cyanea capillata*. Biol Bull 214:29–41

619 Holst S, Sotje I, Tiemann H (2007) Life cycle of the rhizostome jellyfish *Rhizostoma*
620 *octopus* (L.) (Scyphozoa, Rhizostomeae), with studies on cnidocysts and statoliths. Mar
621 Biol 151:1695–1710

622 Jarms G, Morandini AC & Silveira FL (2002) Cultivation of polyps and medusae of
623 Coronatae (Cnidaria, Scyphozoa) with a brief review of important characters. Helgol
624 Mar Res 56:203−210

625 Jaspers C, Titelman J, Hansson, Haraldsson M, Ditlefsen CR (2011) The invasive
626 ctenophore *Mnemiopsis leidyi* poses no direct threat to Baltic cod eggs and larvae.
627 Limnol Oceanogr 56: 431–439

628 Kawahara M, Uye S, Ohtsu K, Iizumi H (2006) Unusual population explosion of the
629 giant jellyfish *Nemopilema nomurai* (Scyphozoa: Rhizostomeae) in East Asian waters.
630 Mar Ecol Prog Ser 307:161–173

631 Koehl MAR (2004) Biomechanics of microscopic appendages: functional shifts caused
632 by changes in speed. J Biomech 37:789–795

633 Koehl MAR, Koseff JR, Crimaldi JP, McCay MG, Cooper T, Wiley MB & Moore PA.
634 (2001) Lobster sniffing: antennule design and hydrodynamic filtering of information in
635 an odor plume. Science 294:1948–1951

636 Kramp P.L. (1970) Zoogeographical studies on Rhizostomeae (Scyphozoa). Vidensk
637 Meddr Dansk Naturh Foren 133:7–30

638 Larson RJ (1991) Diet, prey selection and daily ration of *Stomolophus meleagris*, a
639 filter-feeding scyphomedusa from the NE Gulf of Mexico. Est Coast Shel Sci 32:511–
640 525

641 Lipinski D, Mohseni K (2009) Flow structures and fluid transport for the hydromedusae
642 *Sarsia tubulosa* and *Aequorea victoria.* J Exp Biol 212: 2436−2447.

643 Morandini AC (2003) Estrutura Populacional de *Chrysaora lactea* e *Lychnorhiza*
644 *lucerna* (Cnidaria; Scyphozoa) em amostras de plâncton, com a redescrição das
645 espécies. PhD Dissertation, Universidade de São Paulo, São Paulo, SP

646 Nagata RM, Haddad MA, Nogueira Jr M (2009) The nuisance of medusae (Cnidaria,
647 Medusozoa) to shrimp trawls in central part of southern Brazilian Bight, from the
648 perspective of artisanal fishermen. Pan-Am J Aqua Sci 4:312−325

649 Nagata RM (2015) Bases morfo-funcionais da alimentação e o papel trófico de
650 *Lychnorhiza lucerna* (Scyphozoa, Rhizostomeae). Phd PhD dissertation, Instituto de
651 Biociências da Universidade de São Paulo.

652 Nawroth JC, Feitl KE, Colin SP, Costello JH, Dabiri JO (2010) Phenotypic plasticity in
653 juvenile jellyfish medusae facilitateseffective animal-fluid interaction. Biol Lett
654 6(3):389–393

655 Nogueira Jr M (2006) Macrozooplâncton gelatinoso do litoral do Paraná: Composição,
656 abundância e aspectos ecológicos. Master Dissertation, Universidade Federal do Paraná,
657 Paraná, PR

658 Olesen NJ (1995) Clearance potential of jellyfish *Aurelia aurita*, and predation impact
659 on zooplankton in a shallow cove. Mar Ecol Prog Ser 124:63-72

660 Purcell JE (2009) Extension of methods for jellyfish and ctenophore trophic ecology to
661 large-scale research. Hydrobiologia 616**:**23–50

662 Raskoff KA, Sommer FA, Hamner WM, Cross KM (2003) Collection and culture
663 techniques for gelatinous zooplankton. Biol Bull 204:68-80

664 Riisgård HU (1988) Efficiency of particle retention and filtration rate in 6 species of
665 northeast American bivalves. Mar Ecol Prog Ser 45:217–223

666 Russell FS (1970) The Medusae of British Isles, volume II: Pelagic Scyphozoa.
667 Cambridge University Press

668 Santhanakrishnan A, Dollinger M, Hamlet CL, Colin SP, Miller LA (2012) Flow
669 structure and transport characteristics of feeding and exchange currents generated by
670 upside-down *Cassiopea* jellyfish. J Exp Biol 215:2369-2381

671 Schiariti A, Kawahara M, Uye S-I, Mianzan HW (2008) Life cycle of the jellyfish
672 *Lychnorhiza lucerna* (Scyphozoa: Rhizostomeae) Mar Biol 156:1–12

673 Sugiura Y (1966) On the life-history of rhizostome medusae. IV. *Cephea cephea.*
674 Embryologia 9:105-121

675 Sullivan BK, Suchman C, Costello JH (1997) Mechanisms of prey selection by ephyrae
676 of the scyphomedusa *Aurelia aurita*. Mar Biol 130:213–222

Uchida T (1926) The anatomy and development of a rhizostome medusa, *Mastigias papua* L. Agasiz, with observations on the phylogeny of Rhizostomae. I Fac Sci Tokyo Univ (Sect. 4, Zol.)1:45–95

Vogel S (2003) Comparative Biomechanics: Life's Physical World. Princeton University Press, Princeton

TABLE

Table 1 - Summary of escape response parameters of copepods to feeding currents generated by bell pulsations of *Lychnrohiza lucerna* (0.6-1.5 cm of bell diameter). Means based on 38 escape reactions of *Acartia* spp. and 33 of *Temora turbinata*. Standard error and range are given in parentheses.

Features of escaping response	*T. turbinata* (N=33)	*Acartia* spp (N=38).
Body length of copepod (mm)	0.99 (± 0.19, 0.528-1.28)	1.12 (±0.24, 0.71–1.41)
Distance of reaction (mm)	1.26 (±1.27, 0–6.43)	5.42 (±3.06, 0–11.59)
Jump distance (mm)	10.53 (±5.07, 1.20–20.60)	2.92 (±1.51, 0.96–6.90
Max. velocity of jump ($mm*s^{-1}$)	182.3 (±61.27, 113.21–323.97)	203.28 (±124.11, 80.71–559.67)
Mean turn angle (degrees)	64.90 (±28.24, 8.21-172.13)	28.24 (±22.77, 0-103.34)
Escape angle relative to predator (degrees)	102.74(±50.06, 5.50–176.16)	140.68 (±25.93, 76.08–176.27)
Escape duration (s)	0.12 (±0.06, 0.03-0.28)	0.03 (±0.01, 0.01-0.6)

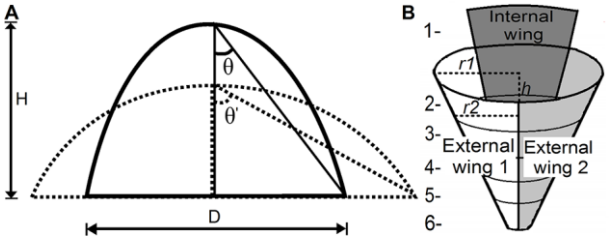

FIGURES

Figure 1 – A. Measurements of bell kinematics. The dotted line is the outline of the bell at the maximum relaxation phase, and the solid line, the outline at the maximum contraction. The dark grey line is the bell angle θ' at the maximum contraction and the light grey dotted line, the bell angle θ at the maximum relaxation. Bell height = H, bell diameter =D at maximum contraction. B. Scheme of the oral arm surface, which comprises three wings (two external and one internal). Each wing was subdivided into regions (5 for the external and 6 for the internal wing) according to the distance from the bell.

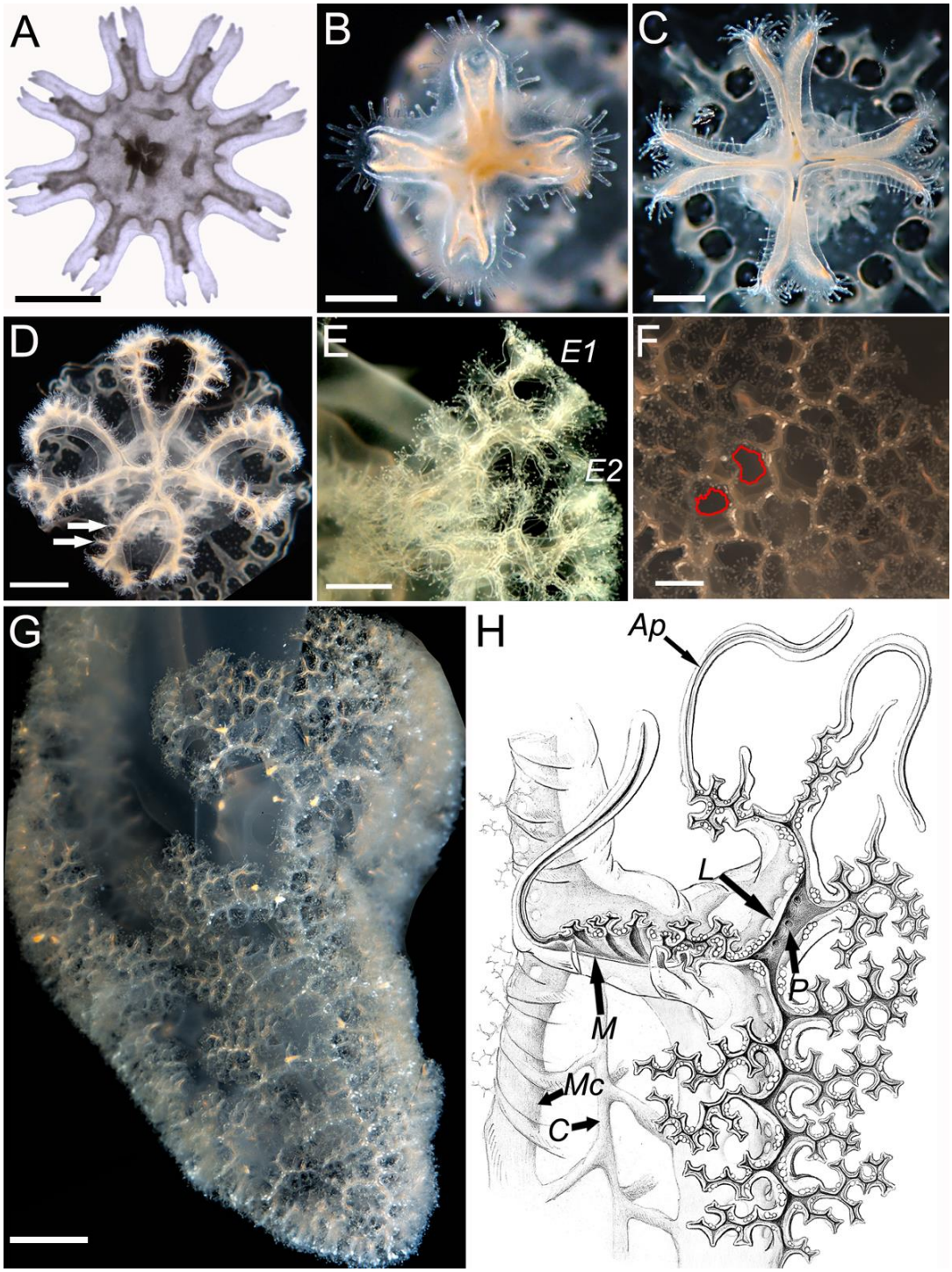

Figure 2 – A. One day-old ephyra with a cross-shaped mouth without *digitata*. B. Mouth of a 5 days old ephyra, with *digitata* along edges. C. Mouth of a 14 days old ephyra, with the oral lips distally divided to eight perradial oral arms. D. 20 days old ephyra, oral arms develops radially, with many lateral folds (arrows), opening of the central mouth still remains. E. The tips of oral arms divide into two external wings (*E1* and E*2*). F. The surface of a fully developed oral arm, with many polygonal gaps (red) through which water & prey are transported. G. The conic-shaped oral arm of a three months old medusa (~3 cm of bell diameter). H. View of the oral arm canal system leading to the small mouths apertures *M*; terminal appendages *Ap*; the small pore of the canal inlet *P*; lateral canals leading to the apertures *L*; main canal of the internal wing *Mc*; the central canal of the oral arm *C*, the *digitata* were not shown. *Scale bar*: A, B and C - 0.5 mm, D – 3 mm, E and F - 1 mm, (G) 3 mm. Illustration: Silvia de Almeida Gonsales.

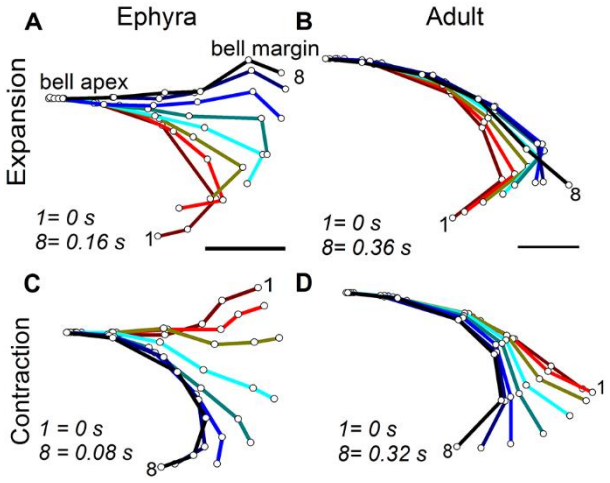

725

726 **Figure 3** – Outlines of half of the bell of *Lychnorhia lucerna* at equall time intervals (1–8), in
727 ephyra (scale = 1 mm), and adult-shaped animal (scale = 10 mm) during bell expansion (A and
728 B) and contraction (C and D).

729

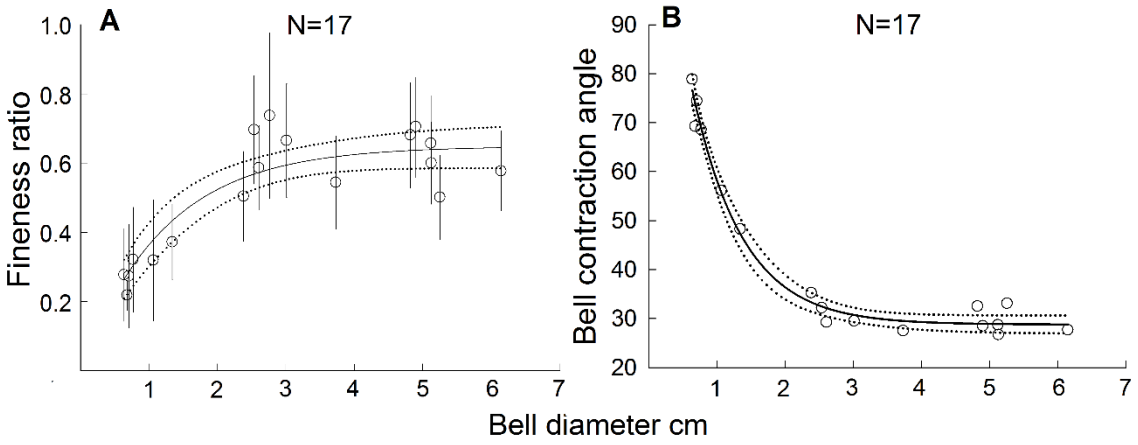

Figure 4 – Bell kinematics of *Lychnorhiza lucerna*. Changes in bell shape were quantified by Fineness ratio f and Bell contraction angle c, along the range of bell diameter (cm). Dotted lines correspond to the 95% confidence intervals for regressions. The regression lines shown are (±95% confidence limits in parentheses) f = 0.65 (±0.03) * (1 - exp(-0.82 (±0.13) * D)) (r^2= 0.81, P<0.001) and c = 28.77 (±0.87) + 113.03 (±11.80) * exp (-1.35 (±0.15)* D) (r^2= 0.98, P<0.001).

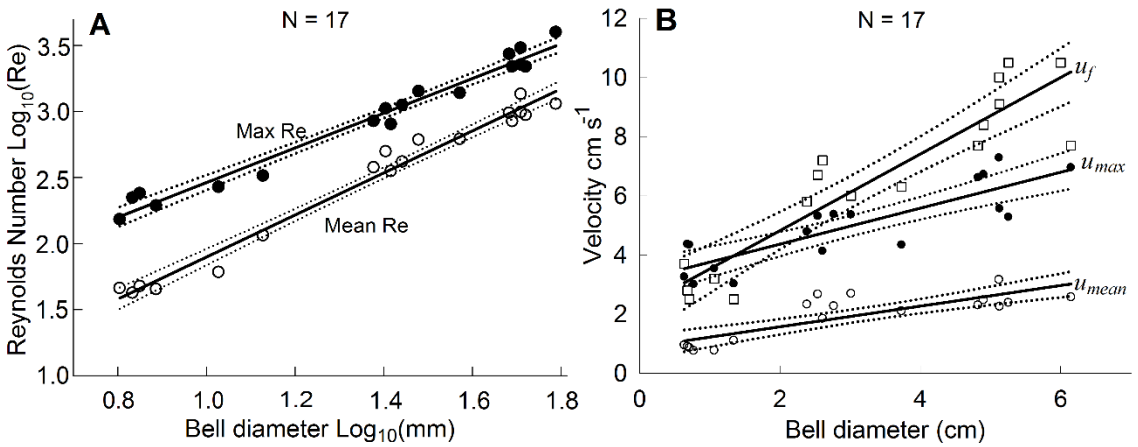

Figure 5 A - Relationship between body size, as bell diameter (mm) and Log_{10} of mean and maximum Reynolds Number Re in *Lychnorhiza lucerna*. B - Relationships between bell diameter of *Lychnorhiza lucerna* and maximun swimming velocity (u_{max}), and mean swimming velocity (u_{mean}), and maximun velocity of feeding currents (u_f). Dotted lines correspond to the 95% confidence intervals for regressions. The regression lines shown are (±95% confidence limits in parentheses): A - Log_{10}Max Re = 1.15 (±0.07) + 1.31 (±0.05) * Log_{10} D (r^2= 0.97, P<0.0001) and Log_{10}Mean Re = 0.31 (±0.08) + 1.59 (±0.05) * Log_{10} D (r^2 = 0.98, P<0.0001); B - u_{max} = 3.15 (±0.31) + 0.61 (±0.09) * D (r^2= 0.73, P<0.0001), u_m = 0.87 (±0.20) + 0.35 (±0.05) * D (r^2= 0.68, P> 0.0001), and u_f = 2.23 (±0.49) + 1.29 (±0.13) * D (r^2= 0.85, P>0.0001).

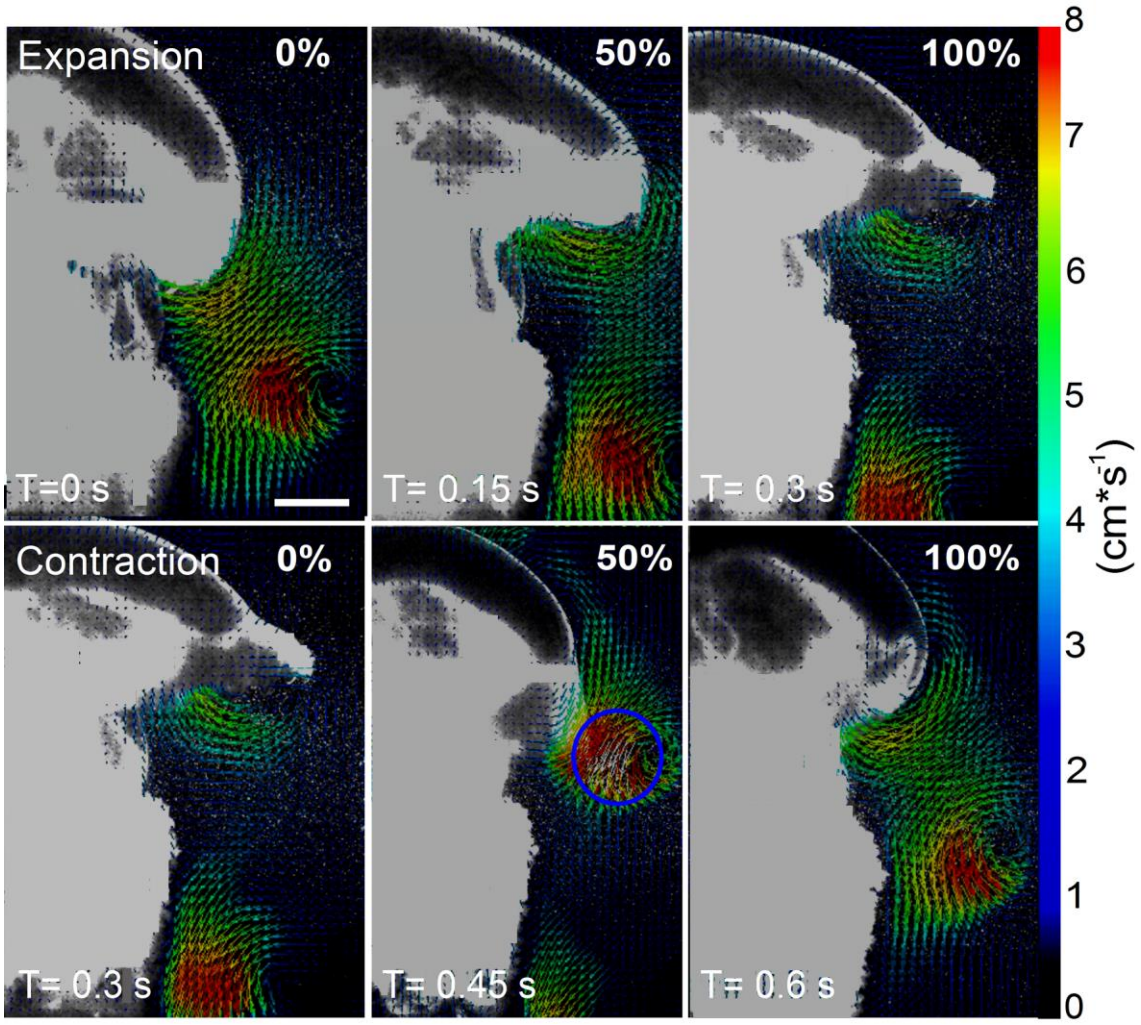

Figure 6– Image sequence of the digital particle image velocimetry (DPIV) technique demonstrating the velocity of fluids (cm*s^{-1}) surrounding a swimming medusa of *Lychnorhiza lucerna*. Figures on top show the expansion phase, when a stopping vortex is formed just below bell margin, and surrounding fluids refill subumbrellar space. Bottom panels demonstrate the contraction phase, when the starting vortex is formed and the highest velocities of the feeding currents (*i.e.* u_f) are shown at 50% (blue circle) of the period of bell contraction. The white vectors at T=0.45 s indicate velocities greater than 8 cm*s^{-1} (~9 cm*s^{-1}). Scale bar = 1 cm.

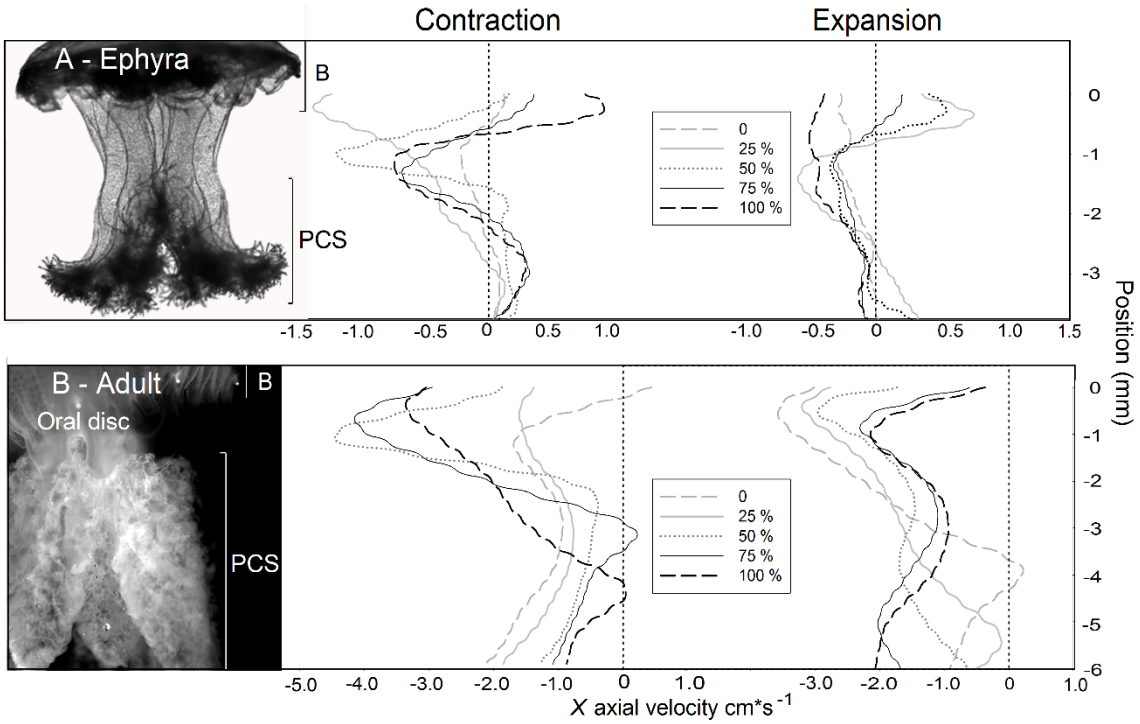

Figure 7 - Axial (*X*) velocities of fluids during both bell contraction and expansion of an ephyra (A) and an adult-shaped medusae (B) of *Lychnorhiza lucerna* of 4 and 26 mm bell diameter. Velocities were measured along a transection from the umbrellar margin to the end of oral arm. Each curve represent the instant velocities taken at 5 time intervals between the start (0) and the end (100%) of both movements. Fluid transport from exumbrella towards the oral arms are represented as negative values, whereas transport from oral arms to outside are positive values. B = bell, PCS = Prey capture surfaces.

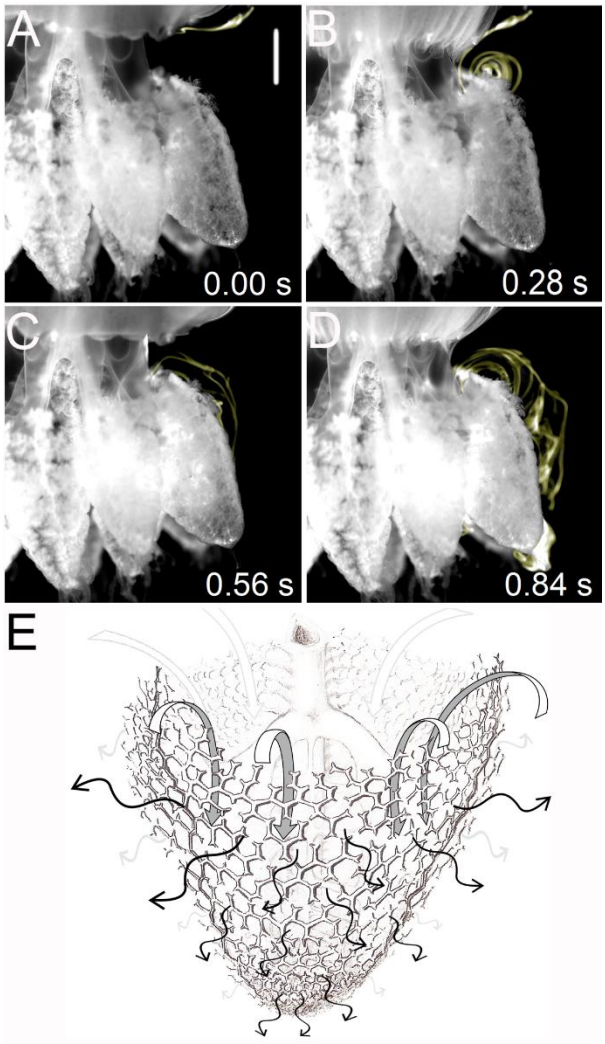

Figure 8 – Sequence of vortice formation during two bell pulsations cycles (**A** – **D**, T= 0.84 s) and interaction of vortex flows with oral arms of *Lychnorhiza lucerna*. Panel **A** shows fluorescein dye been entrained within subumbrellar cavity, below bell margin at the first expansion. Panel **B** shows the subsequent bell contraction and formation of a starting vortex, near the beginning of prey capture surfaces on the oral arms. **C** Shows the next bell expansion and the previous starting vortex translating to inside the oral arms. **D** Shows the next bell contraction and formation of the second starting vortex, while fluid entrained during the first pulsation cycle reaches the tip of the oral arm. **E**- Shows a scheme of the filtration mechanism of an oral arm. Scale bar: 1 cm. Illustration: Silvia de Almeida Gonsales.

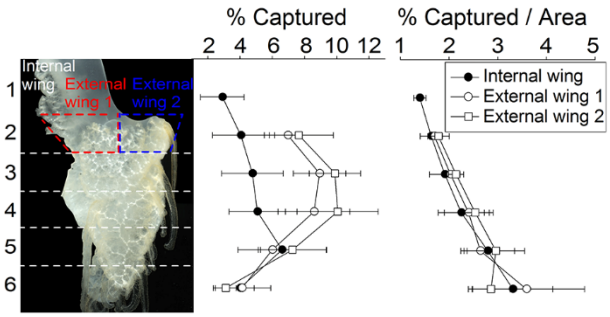

Figure 9 – Map of prey captures along an oral arm of *Lychnorhiza lucerna* (N=5). The three oral wings were divided in regions (1-6 for the internal wing or 2-6 for the external wings) in relation to the distance from the bell. Only the region 1 of the internal wing is shown.

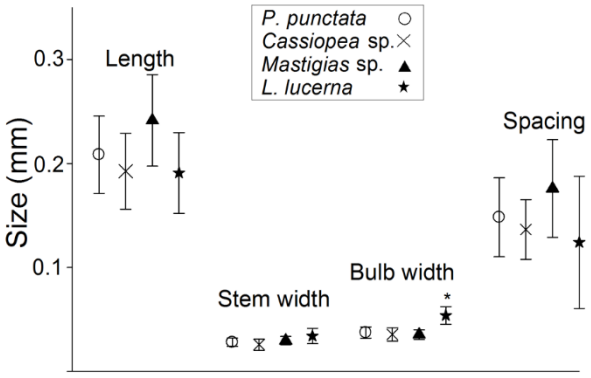

Figure 10 - Morphological features of *digitata* in medusae of Rhizostomeae. A total of 778 measurements were taken, of 3-4 individuals per species (~55 measurements per individual). Among these parameters only the bulb width of *digitata* of *L. lucerna* were significantly larger (ANOVA-NESTED $F_{3,9}$=23.61, * P<0.0001) than other species.